3-15-2014

Patterns of failure in the distal radius following treatment for extra-articular fractures (AO 23-A3.2) using two-column volar plates

Christina Salas

Justin Brantley

James Clark

Evan Baldwin

Mahmoud Reda Taha

See next page for additional authors

Recommended Citation

Christina Salas, Justin Brantley, James Clark, Evan Baldwin, Mahmoud Reda Taha, Deana Mercer. Patterns of failure in the distal radius following treatment for extra-articular fractures (AO 23-A3.2) using two-column volar plates. Poster presented at: ORS 2014 Annual Meeting; Mar 15-18 2014; New Orleans, LA

Authors
Christina Salas, Justin Brantley, James Clark, Evan Baldwin, Mahmoud Reda Taha, and Deana Mercer

Patterns of Failure in the Distal Radius Following Treatment for Extra-Articular Fractures (AO 23-A3.2) Using Two-Column Volar Plates

Christina Salas, MS[1,2]; Justin Brantley, BS[1,2]; James Clark, MD[1]; Evan Baldwin, MD[1,3]; Mahmoud Reda Taha, PhD[2,4]; Deana Mercer, MD[1]

1. Department of Orthopaedics and Rehabilitation
2. Center for Biomedical Engineering 3. Department of Surgery
4. Department of Civil Engineering
The University of New Mexico, Albuquerque, USA

INTRODUCTION

- The distal radius is the most common fracture site in the upper extremity.
- Dorsally displaced, unstable fractures are commonly treated with locked plate fixation using a volar approach.
- Damage analysis of matched paired specimens with simulated AO 23-A3.2 fracture treated with volar plating may provide information on whether implant geometry may affect fracture stability. (Fig. 1)

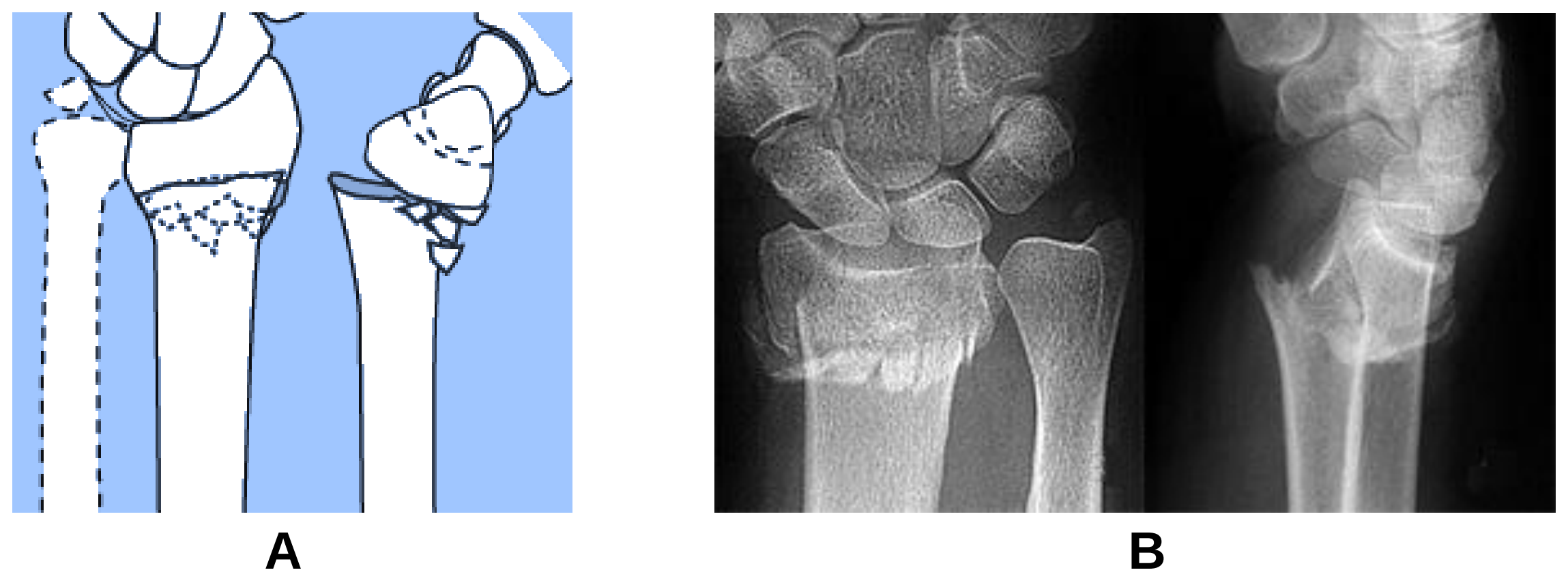

Figure 1: A. Extra-articular multi-fragmentary fracture of the distal radius with angulated dorsal wedge fragment (AO 23-A3.2). B. Radiographic depictions of AO 23-A3.2 fracture.

PURPOSE

- The purpose of our study was to characterize the damage accumulated in a model of extra-articular distal radius fracture with dorsal comminution treated using two-column volar distal radius plates during a simulated post-operative healing period. Patterns of failure of the bone and implant are reported from cyclic testing and ramped load to failure experiments.

METHODS

- Ten matched pairs of fresh-frozen, cadaveric distal radii were used in this study:
    - One radius from each donor was randomized to Group I; the contralateral limb from the same donor assigned to Group II
    - Group I: Prepared with Geminus® volar distal radius plating system by Skeletal Dynamics. (n=10) This implant uses a dual head design for independent two-tier scaffolding. (Fig. 2A)
    - Group II: Prepared with Acu-Loc® 2 Proximal Volar Distal Radius Plate by Acumed. (n=10) This implant uses a single head design for enhanced ulnar butressing. (Fig. 2B)
- A custom fixture was designed to apply a 60/40 ratio through scaphoid and lunate facets. (Fig. 3A)
- Specimens were subject to cyclic axial loading; sinusoidally compressed from 75-250N at a rate of 1 Hz for 5,000 cycles

METHODS

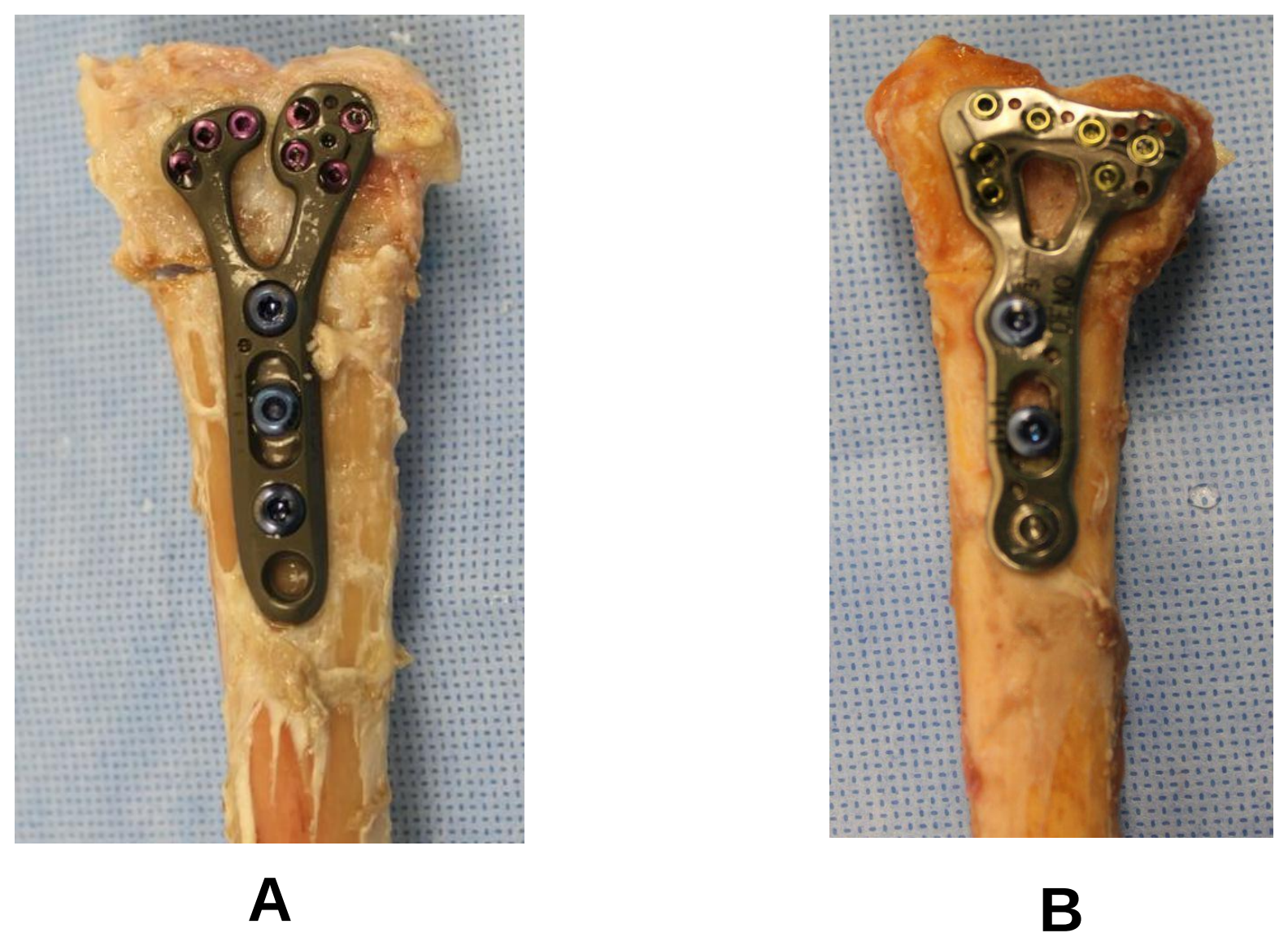

Figure 2: A. Group I radius plated with Geminus® volar distal radius plate from Skeletal Dynamics. B. Group II radius plated with Acu-Loc® 2 proximal volar distal radius plate from Acumed.

- Damage (D), which defines the period between a state of material perfection and the onset of crack initiation, was calculated using the effective Modulus of Elasticity ($E = \frac{PL}{A\Delta}$) from hysteresis data (Fig. 3B)
- $D = 1 - \left[\frac{E\_final}{E\_initial}\right]$, where $E\_initial$ is calculated at cycle 5; E_final is calculated at every 500th cycle
- Constructs not failed during cyclic loading were subject to a ramped load to failure at 1mm/s
- A matched-paired t-test was used to determine statistical significance (p=0.05)

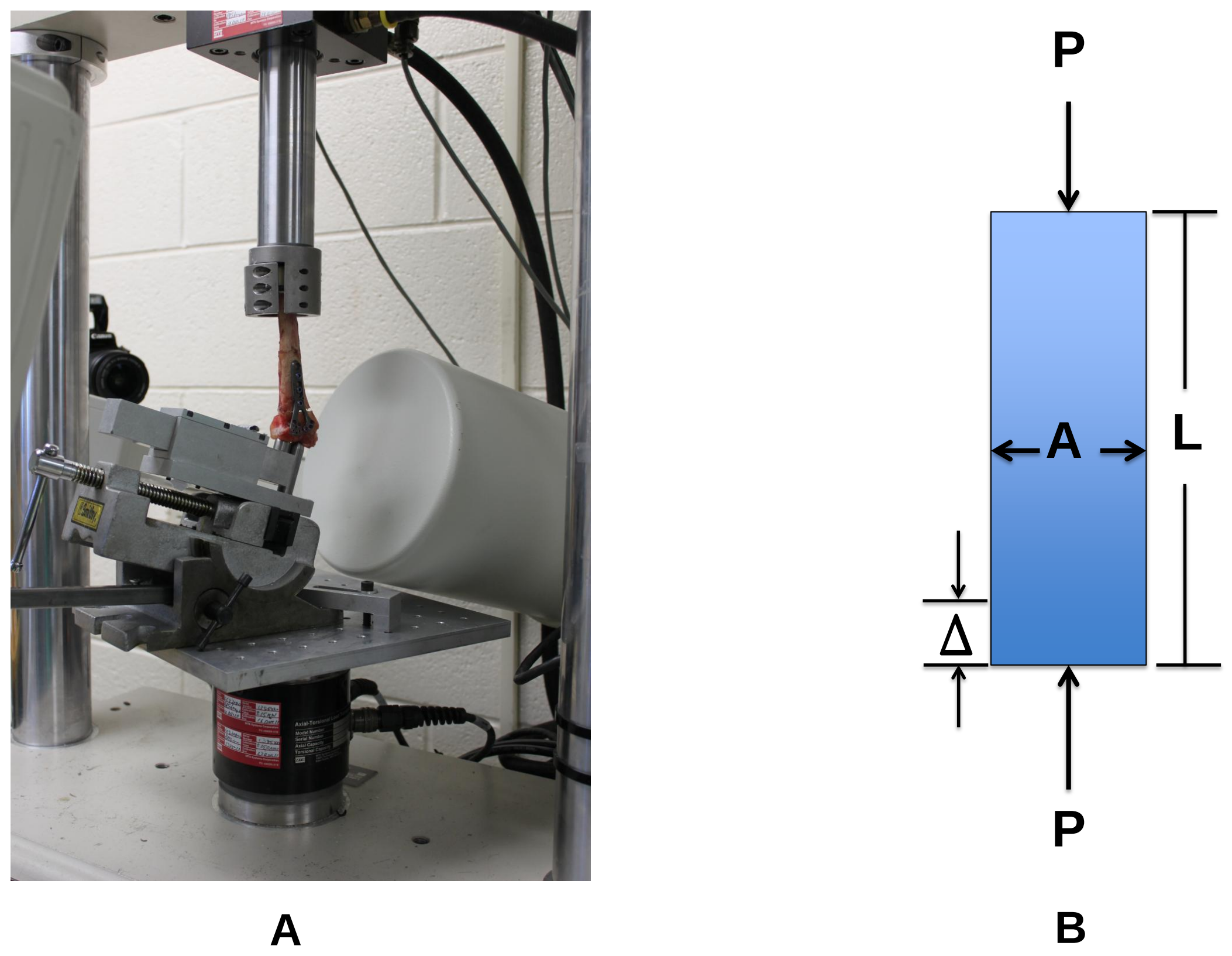

Figure 3: A. Experimental testing fixture. B. Figure depicting axial loading for calculation of effective Modulus of Elasticity.

RESULTS

- Group II specimens experienced significantly more damage under cyclic loading than Group I specimens. (0.78+/-0.11 and 0.66+/-0.10, respectively; p=0.02) (Fig. 4A, Fig. 4B)
- One specimen in Group II experienced coronal fracture of the dorsal pole of the lunate during cyclic loading and was excluded from load to failure tests.
- Group I specimens were significantly stiffer than group II specimens. (481.47+/-161.37 N/mm and 337.90+/-112.04 N/mm, respectively; p=0.04) (Fig. 4C)
- Ultimate force at failure in Group I (1268.50+/-307.69 N) and Group II (1025.63+/-496.45 N) specimens was not significantly different (p=0.11) (Fig. 4D)

RESULTS

- Specimens failed by distal fragment collapse leading to plate bending (Group I n=5/10; Group II n=2/9) and fracture of the lunate facet (Group I n=5/10; Group II n=7/9)

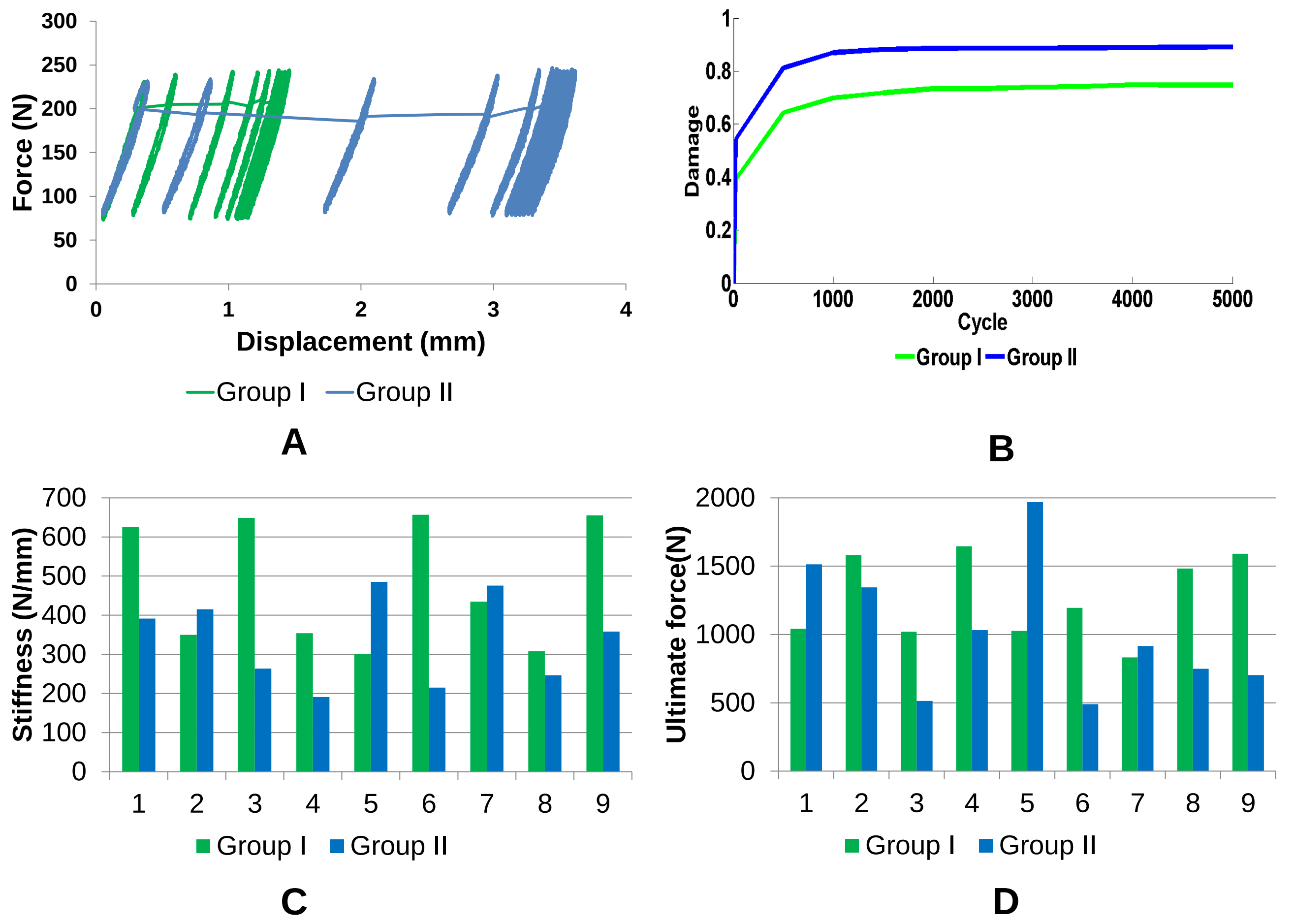

Figure 4: A. Representative force-displacement hysteresis curves of a single specimen from Group I and contralateral limb in Group II. B. Representative damage plots. C. Stiffness results from load-to-failure testing. D. Ultimate failure force results from load-to-failure testing.

CONCLUSIONS

- Structural damage, though greater in Group II specimens during low cycle loading, did not significantly affect the ultimate failure force of the bone/implant constructs
- In order to determine the cause of the low-cycle structural damage to Group I and Group II specimens, a patient-specific computational analysis is underway, developed using pre-study calibrated quantitative computed tomography scans of the bones and solid models of the implants

CLINICAL RELEVANCE

- If a patient is subject to high impact loading of the distal radius (fall on outstretched hand) prior to the end of their post-operative healing period, both implants may provide equivalent resistance to fracture
- Should the post-operative healing period be delayed, it is likely that increasing damage may lead to fracture with Group II implants; high frequency fatigue testing is necessary to confirm

ACKNOWLEDGEMENTS

- This project was supported in part by the National Center for Advancing Translational Sciences of the National Institutes of Health through grant number UL1 TR000041. The content does not necessarily represent the official views of the NIH.